Korean J. Chem. Eng., 40(8), 2010-2016 (2023)
DOI: 10.1007/s11814-023-1464-5

pISSN: 0256-1115
eISSN: 1975-7220

A novel fluorescent turn-on probe based on thiosemicarbazide-naphthalene for selectively detecting Zn^{2+}

Minji Lee, Sungjin Moon, Dongkyun Gil, and Cheal Kim†

Department of Fine Chemistry, and New and Renewable Energy Convergence, Seoul National University of Science and Technology, Seoul 01811, Korea
(*Received 4 January 2023 • Revised 3 March 2023 • Accepted 31 March 2023*)

Abstract−A new thiosemicarbazide-naphthalene-based fluorescent chemosensor **FNC** ((2-(furan-2-carbonyl)-N-(naphthalen-1-yl)hydrazine-1-carbothioamide)) for Zn^{2+} was synthesized and identified. **FNC** was applied to selectively detect Zn^{2+} with fluorescent turn-on response. The detection limit was determined to be 1.93 μM, which is much below the WHO standard (76.5 μM). The detecting mechanism of **FNC** to Zn^{2+} was revealed to bind **FNC** to Zn^{2+} in the proportion of 1 : 1 by Job plot, ESI-mass and ^{1}H NMR titrations. DFT and TD-DFT calculations were performed for **FNC** and **FNC**-Zn^{2+}, which provide insight into structural, electronic and photophysical properties.

Keywords: Thiosemicarbazide, Naphthalene, Fluorescence Chemosensor, Zn(II), TD-DFT Calculations

INTRODUCTION

Metal contamination has become a serious hazard to living organisms and human health due to the inevitable release of metal ions from human activities like coal burning, mining, metal refining and steel production [1-6]. In particular, zinc is the second common metal in the organism system [7-12]. Zinc ion (Zn^{2+}) plays an essential role in the maintenance of homeostasis, cell viability and neuronal signal transduction [13-15]. On the other hand, non-ideal amounts of Zn^{2+} in organisms cause neurodegenerative diseases like Alzheimer's disease and Wilson's disease [16-20]. Therefore, developing analytical tools with a simple way for selective Zn^{2+} detection has become increasingly important.

Many methods have been used for sensing Zn^{2+}, like ion chromatography, mass spectrometry, atomic absorption spectroscopy and fluorescence spectrometry [21-26]. Among those methods, fluorescence chemosensor has various advantages due to easy detection, portability, cost-benefit, high selectivity, real-time responses and low detection limit [27-34]. According to the advantages, several fluorophores have been used to detect Zn^{2+}, such as quinoline, benzimidazole, benzofuran, naphthalene and fluorescein [35-38]. However, due to their poor water-solubility, it is still challenging to develop chemosensors detecting Zn^{2+} in an aqueous solution [39-41]. Therefore, water-soluble moiety needs to be introduced to the chemosensors. Moreover, many fluorescent chemosensors for Zn^{2+} have difficulty in the discrimination of Zn^{2+} from Cd^{2+} [42-45]. Therefore, it is important to invent fluorescent chemosensors capable of discriminating Zn^{2+} from Cd^{2+}.

Thiosemicarbazide has selective binding sites for metal ions because its three nitrogen atoms provide lone-pair electrons with the metal ions such as Zn^{2+} [46-49]. Moreover, thiosemicarbazide has a good water-soluble property [50]. On the other hand, naphthalene moiety could serve as a fluorescence signaling group [51,52]. In this regard, the chemosensor derived from the combination of naphthalene and thiosemicarbazide is expected to detect Zn^{2+} by the fluorescence variation in an aqueous solution.

Herein, we report a thiosemicarbazide-naphthalene-based fluorescent chemosensor **FNC** for Zn^{2+} detection. **FNC** showed a significant increase in fluorescence upon the addition of Zn^{2+} and could discriminate Zn^{2+} from Cd^{2+}. In addition, it was proven that **FNC** bound with Zn^{2+} in the proportion of 1 : 1 by Job plot, ESI-MS and ^{1}H NMR titrations. The fluorescence enhancement of **FNC** by the complexation of **FNC** with Zn^{2+} was studied by DFT and TD-DFT calculations.

EXPERIMENTS

1. Materials and Equipment

Reagents used for all experiments were provided commercially. NMR spectra were recorded by a Varian spectrometer. Fluorescence and UV/Visible absorption spectra were obtained by using Perkin Elmer spectrometers (LS45 and Lambda 25). A single-quadrupole ACQUITY QDa was used for ESI-mass data.

2. Synthesis of FNC (2-(furan-2-carbonyl)-N-(naphthalen-1-yl)hydrazine-1-carbothioamide)

Furan-2-carbohydrazide (1 mmol, 126 mg) and 1-isothiocyanatonaphthalene (1 mmol, 185 mg) reacted in 15.0 mL of ethanol for 3 h at 20 °C. This mixture was stirred until a pale white powder precipitated. The pale white powder obtained was washed with icy ethanol and diethyl ether. Yield: 258 mg (83%). ^{1}H NMR (400 MHz, DMF-d_7): δ (ppm)=10.79 (s, 1H, NH), 10.29 (s, 1H, NH), 9.81 (s, 1H, NH), 8.12 (m, 1H, A^a-H), 7.95 (m, 2H, A^a-H), 7.87 (d, J=8.0 Hz, 1H, A^b-H), 7.51 (m, 4H, A^a-H), 7.32 (d, J=3.6 Hz, 1H, A^b-H), 6.70 (m, 1H, A^b-H) (A^a=naphthalene, A^b=thiophene). ^{13}C NMR (175 MHz, DMSO-d_7): δ=182.4, 157.7, 146.5, 145.5, 135.7, 133.6, 127.72, 126.7, 126.3, 125.9, 125.7, 125.3, 123.8, 114.7, 111.7

†To whom correspondence should be addressed.
E-mail: chealkim@snut.ac.kr

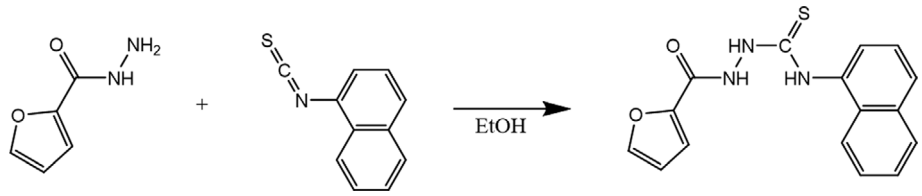

Scheme 1. Synthesis of FNC.

ppm. ESI-Mass: m/z cacld. for $[C_{16}H_{14}N_3O_2S+K^+]^+$: 350.04; found, 349.95.

3. Fluorescent and UV-vis Titrations

FNC (1.6 mg, 5.0 μmol) was dissolved in 500 μL DMF (dimethylformamide) to produce 10 mM, and 6.0 μL of the **FNC** stock was diluted in 2.994 mL of bis-tris buffer/DMF (9 : 1, pH=7.0, 10 mM) to afford 20 μM. $Zn(NO_3)_2$ (11.4 mg, 60 μmol) was dissolved in 3.0 mL of DMF to produce 20 mM. 0.6-9.0 μL of the $Zn(NO_3)_2$ stock was progressively poured into **FNC** solutions. Fluorescent and UV-vis spectra were recorded after 10 s.

4. Job Plot

0.1 mL of a **FNC** stock (10 mM) was diluted to 19.9 mL of a mixture of buffer/DMF (9 : 1) to provide 50 μM. 0.05 mL of a $Zn(NO_3)_2$ stock (20 mM) was diluted to 19.5 mL of bis-tris buffer/DMF (9 : 1) to provide 50 μM. 0.3-2.7 mL of the diluted Zn(II) and 2.7-0.3 mL of the diluted **FNC** were mixed respectively to make 3 mL of solutions. Fluorescent spectra were recorded after 10 s.

5. Competitive Experiments

60 μmol of $Al(NO_3)_3$, $Cu(NO_3)_2$, $Cr(NO_3)_3$, $Pb(NO_3)_2$, $Hg(NO_3)_2$, $Co(NO_3)_2$, $Ni(NO_3)_2$, $Ca(NO_3)_2$, $Mg(NO_3)_2$, $Mn(NO_3)_2$, $In(NO_3)_3$, $Ga(No_3)_2$, $NaNO_3$, $AgNO_3$, $Fe(NO_3)_3$, $Fe(ClO_4)_2$, $Cd(NO_3)_2$, and KNO_3 was, respectively, dissolved in 3.0 mL of bis-tris buffer/DMF (9 : 1). 9 μL of the respective metal was separately diluted to 3.0 mL of bis-tris buffer/DMF (9 : 1) to provide 3.0 equiv. 9.0 μL of a Zn(II) stock (20 mM) was added to the solutions, respectively. Fluorescent spectra were recorded after 10 s.

6. pH Test

Bis-tris buffers (10 mM) with pH values (6.0-9.0) were prepared by adding HCl and NaOH in buffer solutions. 6 μL of a **FNC** stock (10 mM) was diluted to 2.994 mL of buffer/DMF (9 : 1) with pH values ranging from 6-9. Fluorescent emission of **FNC** with various pH values was recorded. 9.0 μL of a Zn(II) stock (20 mM) was added to the solutions having diverse pH values to give 3.0 equiv. Fluorescent emission spectra of the solutions were recorded at each pH after 10 s.

7. Determination of Zn^{2+}

Fluorescence analysis of Zn^{2+} in real water samples was conducted by adding 6.0 μL of a **FNC** stock (10 mM) and 2.7 mL of buffer to 0.3 mL of samples. Fluorescent spectra were recorded after 10 s.

8. Test Strips Towards Zn^{2+}

An **FNC** stock (10 mM) was prepared in DMSO. By immersing the filter papers into the **FNC** solution and drying them in the oven, the fluorescent test strips were obtained. Stock solutions (100 μM) of various metal ions were prepared in buffer/DMF (9 : 1). The test strips of **FNC** were added to the metal solutions and then dried.

9. DFT Calculation Methods

We carried out density functional theory (DFT) calculations with Gaussian 16 program [53]. The calculations were implemented with B3LYP [54] functional and the 6-31G(d,p) basis set [55,56]. Lanl2DZ [57] effective core potential was used for Zn^{2+}. The solvent effect of DMF was considered by using IEFPCM [58]. In vibrational frequency calculations, the imaginary frequency did not appear, suggesting that the optimized **FNC** and **FNC**-Zn^{2+} represented local minima.

RESULTS AND DISCUSSION

As shown in Scheme 1 the probe **FNC** was synthesized by the reaction of furan-2-carbohydrazide and 1-isothiocyanatonaphthalene in EtOH. Compound **FNC** was verified by ^1H and ^1C NMR (Figs. S1 and S2) and ESI-MS (Fig. S3). The detection of Zn^{2+} by **FNC** was explained by fluorescent and UV-vis spectroscopy, ^1H NMR titration and theoretical calculations.

1. Spectroscopic Studies of Probe FNC with Zn^{2+}

The selective detecting ability of **FNC** for Zn^{2+} was examined by analyzing the fluorescent spectral changes of **FNC** with Zn^{2+} and other metal ions (Al^{3+}, Cu^{2+}, Cr^{3+}, Pb^{2+}, Hg^{2+}, Co^{2+}, Ni^{2+}, Ca^{2+}, Mg^{2+}, Mn^{2+}, In^{3+}, Ga^{2+}, Na^+, Ag^+, Fe^{3+}, Fe^{2+}, Cd^{2+} and K^+) in bis-tris buffer/DMF (9 : 1) (Fig. 1). With excitation at 350 nm, only Zn^{2+} induced a prominent increase in emission intensity at 440 nm. Except for some increase in the emission spectrum of **FNC** with silver ions, no significant change in emission spectra of **FNC** with other metal ions was observed. These results verified that probe **FNC** could be a fluorescent turn-on chemosensor for detecting Zn^{2+}

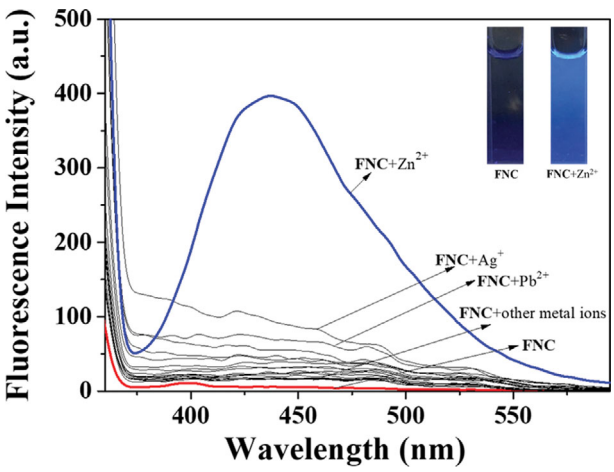

Fig. 1. Florescent changes of FNC (2×10^{-5} M) with various cations (3.0 equiv).

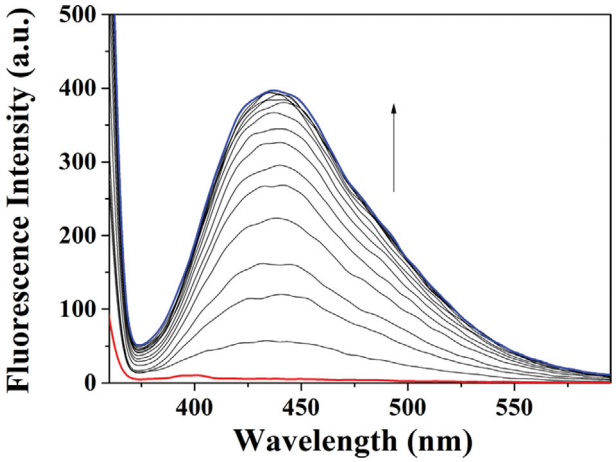

Fig. 2. Fluorescent changes of FNC (2×10^{-5} M) with different concentrations of Zn^{2+} (0-3.0 equiv).

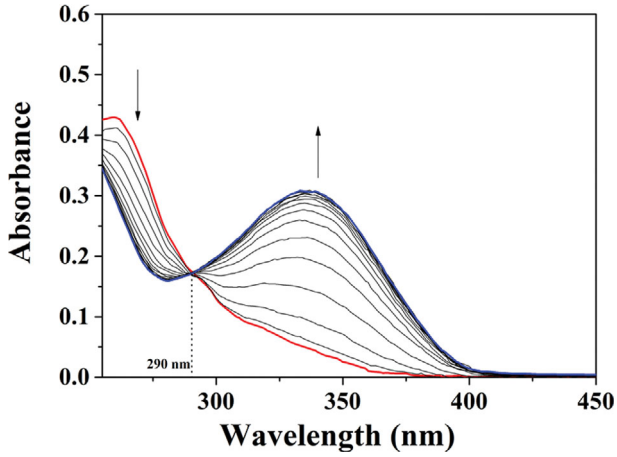

Fig. 3. UV-vis changes of (2×10^{-5} M) with different concentrations of Zn^{2+} (0-3.0 equiv).

selectively and discriminating Zn^{2+} from Cd^{2+}.

Fluorescence and UV-vis titrations were performed to demonstrate a reaction process of **FNC** to Zn^{2+}. When Zn^{2+} was added to **FNC**, the fluorescent intensity at 440 nm increased significantly until the addition of 3.0 equiv of Zn^{2+} (Fig. 2). Quantum yields (Φ) of **FNC** and **FNC**-Zn^{2+} turned out to be 0.0324 and 0.5796 [59]. In the UV-vis titration, absorbance at 333 nm increased, while absorbance at 260 nm decreased by adding Zn^{2+} into **FNC** (Fig. 3). The UV-vis spectrum showed an isosbestic point at 290 nm, meaning that the binding reaction of **FNC** with Zn^{2+} makes only one species.

To identify the binding ratio of **FNC** with Zn^{2+}, a Job plot was implemented and analyzed (Fig. S4). The maximum intensity value was measured at 0.5 of $[Zn^{2+}]/([\mathbf{FNC}]+[Zn^{2+}])$, implying that the complex of **FNC**-Zn^{2+} was made in the proportion of 1 : 1. In addition, ESI-mass data was recorded to verify the 1 : 1 complex formation of **FNC**-Zn^{2+} (Fig. S5). The peak of 455.94 (m/z) was assigned as $[\mathbf{FNC}–H^{+}+Zn^{2+}+2\cdot MeCN]^{+}$ (calcd. m/z=456.05). The result supported the 1 : 1 binding mechanism of **FNC** with Zn^{2+}. The limit of detection was calculated to be 1.93 μM by using $C_{DL}=3\sigma/k$ (Fig. S6). It is far below the WHO standard for Zn^{2+} (76.5 μM). The binding constant (K) of 2.9×10^{5} M^{-1} was gained by using the non-linear fitting method (Fig. S7).

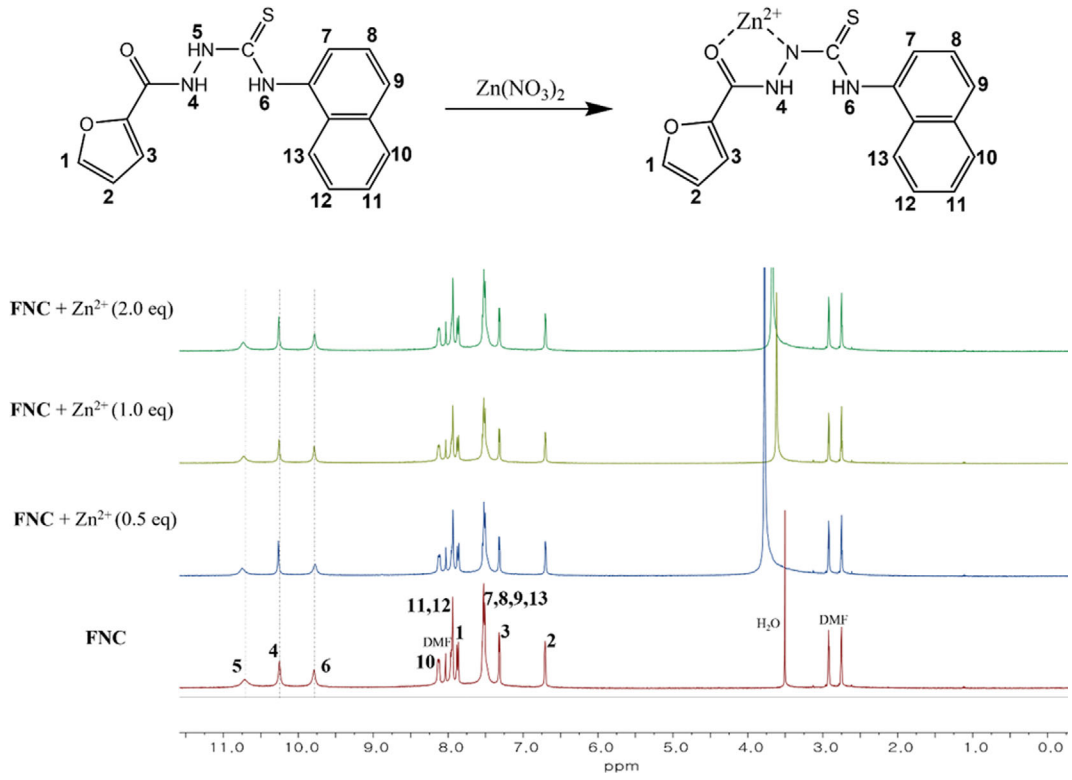

Fig. 4. ^{1}H NMR titration of FNC with Zn^{2+} (0, 0.5, 1.0 and 2.0 equiv).

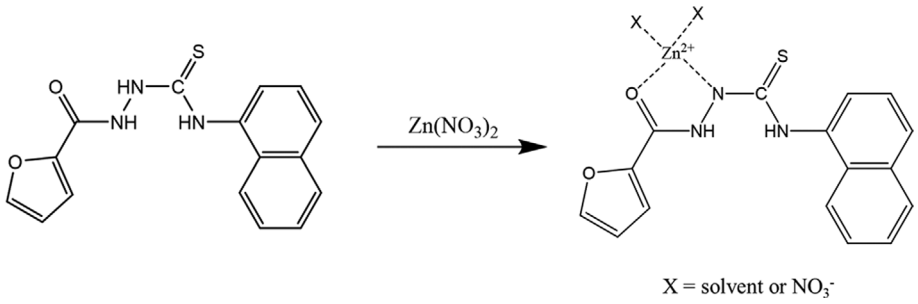

Scheme 2. Proposed structure of FNC-Zn^{2+}.

Moreover, we implemented ^{1}H NMR titration to understand the sensing mechanism of **FNC** to Zn^{2+} (Fig. 4). When 2.0 equiv of Zn^{2+} were added to the **FNC** solution, the integral value of the proton H_5 decreased by half. The proton H_4 slightly shifted downfield. The changes confirmed that zinc ion might bind to nitrogen of the thiosemicarbazide and the carbonyl oxygen. We further identified the binding structure by FT-IR (Fig. S8). Upon binding of Zn^{2+} to **FNC**, the band at 3,332 cm^{-1} associated with one amine group of **FNC** disappeared, and the band associated with the C=O peak moved significantly from 1,682 cm^{-1} to 1,519 cm^{-1}. On the other hand, the C=S peak at 763 cm^{-1} showed a slight shift to 748 cm^{-1}. These results indicated that the O atom of the C=O moiety might participate in the coordination bond with Zn^{2+}. Considering all the outcomes of the Job plot, ESI-MS, ^{1}H NMR titrations and FT-IR, we suggested the binding structure of **FNC** with Zn^{2+} (Scheme 2).

Competitive experiments were implemented to verify the detecting capability of **FNC** to Zn^{2+} in the existence of other cations (Fig. S9). When **FNC** was dealt with both zinc ion and other competitive metal ions, the fluorescence intensities for all other metal ions diminished by 35 to 62%. However, the fluorescence was sufficiently strong to be visible. Moreover, a pH test was carried out to demonstrate the practical usability of chemosensor **FNC** (Fig. 5). **FNC** showed intense fluorescence at pH 7, 8 and 9 when 3.0 equiv of Zn^{2+} was added.

To examine the practical capability of **FNC**, the application of **FNC** was achieved in both tap and drinking water samples (Table 1). Reasonable R.S.D. values and recoveries were obtained. The results signified that **FNC** could be a practical tool for detecting Zn^{2+} in real water samples. To further inspect the practical utility of **FNC**, test strips of **FNC** were prepared by immersing the filter papers in a **FNC** stock. When the test strips coated with **FNC** were soaked with various cations, a fluorescence change was observed only for Zn^{2+}, showing the blue fluorescence (Fig. 6). Therefore,

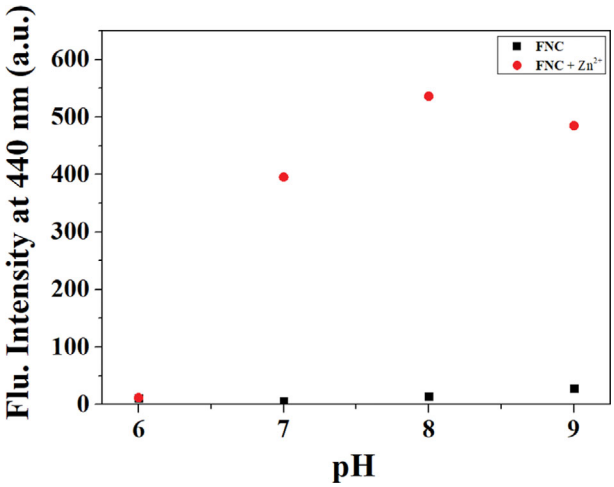

Fig. 5. Fluorescence emissions of FNC at pH 6-9 on the addition of Zn^{2+}.

the test strips coated with **FNC** would be useful for detecting Zn^{2+}. Importantly, **FNC** is the first thiosemicarbazide-based fluorescent chemosensor for Zn^{2+} that could be successfully applied to both real water samples and test strips (Table S1).

2. DFT Calculations

To understand the fluorescence sensing of **FNC** to Zn^{2+}, DFT calculations were carried out. The energy-minimized structures of **FNC** and **FNC**-Zn^{2+} are shown in Fig. 7. The structure of **FNC** has a dihedral angle of 16.885° (1N, 2N, 3C and 4N) with a folded conformation structure. The structure of **FNC**-Zn^{2+} has a dihedral angle of 11.42° with a relatively flatted form. The complexation of **FNC** with Zn^{2+} causes the structure of **FNC** to be more planar and rigid.

We implemented TD-DFT calculations with the optimized forms to comprehend the electronic transitions of the singlet excited

Table 1. Determination of Zn^{2+}[a]

Sample	Zn^{2+} added (μM)	Zn^{2+} found (μM)	Recovery (%)	R.S.D. (n=3) (%)
Tap water	0.0	0.0	-	-
	10.0	10.26	102.3	0.05
Drinking water	0.0	0.0	-	-
	10.0	10.23	102.6	0.74

[a]Conditions: [**FNC**]=2×10^{-5} M in bis-tris buffer/DMF (9 : 1)

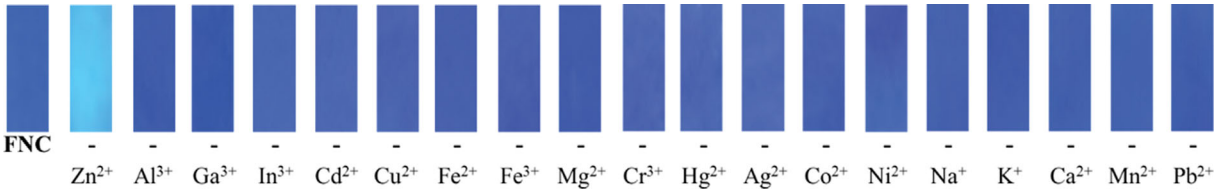

Fig. 6. FNC-coated test strips applied to Zn^{2+} (100 μM) and varied cations.

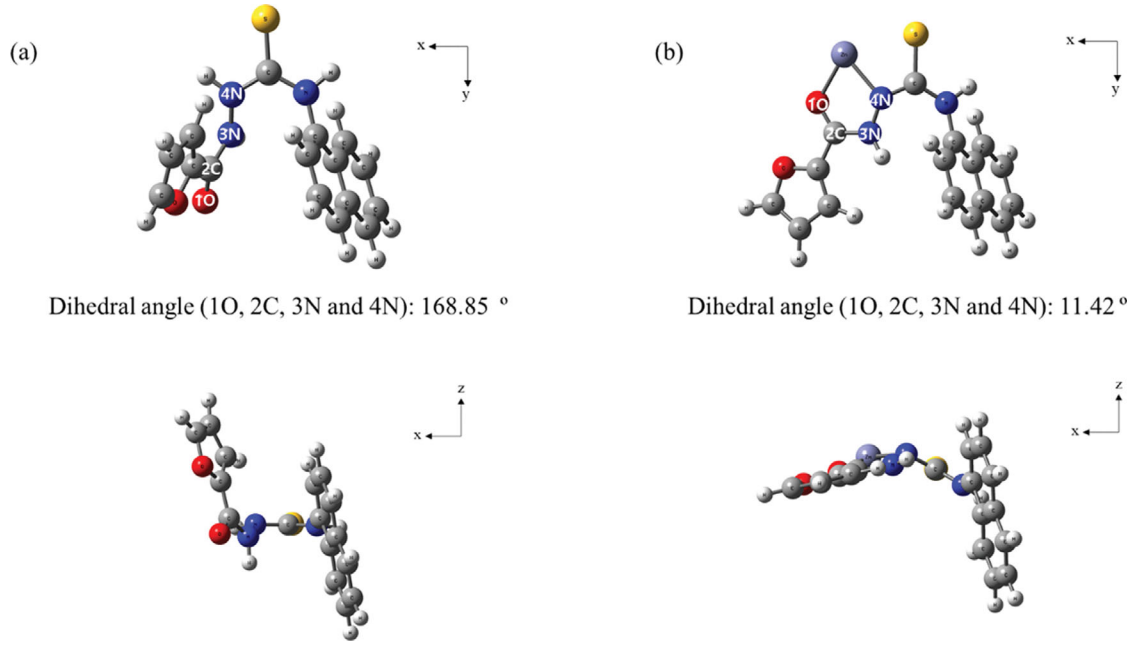

Fig. 7. The energy-minimized features of (a) FNC and (b) FNC-Zn^{2+}.

states for **FNC** and **FNC**-Zn^{2+}, respectively. For **FNC**, the major molecular orbital (MO) contribution of the excited state 1 (306.95 nm) was determined for the HOMO to LUMO (47%) and the HOMO-1 to LUMO (35%) transitions, which showed the ICT process and π-π* transition (Figs. S10 and S11). The electron cloud moved from the thiocarbonyl group to the furan group and π-π* transition appeared in the naphthyl group. For **FNC**-Zn^{2+}, the main MO contribution of the excited state 1 (351.11 nm) was assigned as the HOMO to LUMO, which showed the LMCT and π-π* transitions (Figs. S11 and S12). After binding with Zn^{2+}, the electron cloud of **FNC** shifted to Zn^{2+} due to the electron-withdrawing ability of Zn^{2+}. The π-π* transition of the naphthyl group was similar to that of free **FNC**. The LMCT effect of **FNC**-Zn^{2+} induced the decrement of the band-gap energy of the ground and excited energy levels (4.10 eV for **FNC**-Zn^{2+} and 4.62 eV for **FNC**). The change of computed UV-vis absorption (291.07 nm to 317.04 nm) caused by the complexation coincided with the redshift in the experimental UV-vis spectra (295 nm to 333 nm). Thus, we could suggest that the structural rigidity of **FNC**-Zn^{2+} would lead to the enhancement of fluorescence by the CHEF effect.

CONCLUSION

We developed a thiosemicarbazide-based fluorescent probe **FNC** for selectively detecting Zn^{2+}. **FNC** with Zn^{2+} showed intense blue-fluorescence even though Zn^{2+} coexisted with other metal ions. **FNC** has a detection limit of 1.93 μM, which is much below the WHO standard. The **FNC**-Zn^{2+} coordination properties were demonstrated by Job plot, ESI-mass and ^{1}H NMR titrations. It was revealed that **FNC** could bind with Zn^{2+} in the proportion of 1 : 1. Based on DFT and TD-DFT calculations, we propose that the structural rigidity and the energy band-gap decrease caused by the complexation of **FNC**-Zn^{2+} induced the enhancement of fluorescence.

ACKNOWLEDGEMENT

The National Research Foundation of Korea (2018R1A2B6001686) is gratefully acknowledged.

SUPPORTING INFORMATION

Additional information as noted in the text. This information is available via the Internet at http://www.springer.com/chemistry/journal/11814.

REFERENCES

1. J. Briffa, E. Sinagra and R. Blundell, *Heliyon*, **6**, e04691 (2020).

2. M. Ariannezhad, D. Habibi, S. Heydari and V. Khorramabadi, *Korean J. Chem. Eng.*, **38**, 1510 (2021).
3. M. Theetharappan and M. A. Neelakantan, *J. Fluoresc.*, **31**, 1277 (2021).
4. P. Cheng, Y. Ren, L. Yang, R. Li, X. Wang, B. Li and H. Yuan, *Korean J. Chem. Eng.*, **39**, 3350 (2022).
5. Z. Long, Y. Huang, W. Zhang, Z. Shi, D. Yu, Y. Chen, C. Liu and R. Wang, *Environ. Monit. Assess.*, **193** (2021).
6. J. M. Jung, C. Kim and R. G. Harrison, *Sens. Actuators B Chem.*, **255**, 2756 (2018).
7. A. Pandith, N. Uddin, C. H. Choi and H. S. Kim, *Sens. Actuators B Chem.*, **247**, 840 (2017).
8. H. Xu, C. Zhu, Y. Chen, Y. Bai, Z. Han, S. Yao, Y. Jiao, H. Yuan, W. He and Z. Guo, *Chem. Sci.*, **11**, 11037 (2020).
9. D. Maity and T. Govindaraju, *Chem. Commun.*, **48**, 1039 (2012).
10. D. Choe and C. Kim, *J. Chem. Sci.*, **133** (2021).
11. X. Wu, Z. Zhang, H. Liu and S. Pu, *RSC Adv.*, **10**, 15547 (2020).
12. D. Xiang, S. Zhang, Y. Wang, K. Sun and H. Xu, *Tetrahedron*, **106-107**, 132648 (2022).
13. B. Suh, D. Gil, S. Yoon, K.-T. Kim and C. Kim, *Chemosensors*, **10**, 32 (2022).
14. Y. P. Zhang, W. Y. Niu, C. M. Ma, Y. S. Yang, H. C. Guo and J. J. Xue, *Inorg. Chem. Commun.*, **130**, 108735 (2021).
15. M. Mary Mathew and A. Sreekanth, *Inorg. Chim. Acta*, **516**, 120149 (2021).
16. J. B. Chae, D. Yun, S. Kim, H. Lee, M. Kim, M. H. Lim, K. T. Kim and C. Kim, *Spectrochim. Acta A Mol. Biomol. Spectrosc.*, **219**, 74 (2019).
17. M. Kiani, M. Bagherzadeh, S. Meghdadi, N. Rabiee, A. Abbasi, K. Schenk-Joß, M. Tahriri, L. Tayebi and T. J. Webster, *New J. Chem.*, **44**, 11841 (2020).
18. M. Ruz, F. Carrasco, P. Rojas, K. Basfi-fer, M. C. Hernández and A. Pérez, *Biol. Trace Elem. Res.*, **188**, 177 (2019).
19. J. Y. Yun, T. G. Jo, J. Han, H. J. Jang, M. H. Lim and C. Kim, *Sens. Actuators B Chem.*, **255**, 3108 (2018).
20. J. H. Kang and C. Kim, *Photochem. Photobiol. Sci.*, **17**, 442 (2018).
21. M. K. Swami and P. K. Gupta, *Proc. Natl. Acad. Sci. India Sect. A - Phys. Sci.*, **88**, 453 (2018).
22. N. A. S. Pungut, H. Mat Saad, K. S. Sim and K. W. Tan, *J. Photochem. Photobiol. A Chem.*, **414**, 113290 (2021).
23. S. Anbu, A. Paul, K. Surendranath, N. S. Solaiman and A. J. L. Pombeiro, *Sens. Actuators B Chem.*, **337**, 129785 (2021).
24. P. Bhalla, A. Goel, N. Tomer and R. Malhotra, *Inorg. Chem. Commun.*, **136** (2022).
25. M. X. Lv, L. Y. Bian, W. N. Wu, Z. H. Xu, Y. Wang, X. L. Zhao, Z. Q. Xu, Y. C. Fan and L. L. Yan, *Color. Technol.*, 1 (2021).
26. N. A. S. Pungut, M. P. Heng, H. M. Saad, K. S. Sim, V. S. Lee and K. W. Tan, *J. Mol. Struct.*, **1238**, 130453 (2021).
27. D. Y. Lee, N. Singh and D. O. Jang, *Tetrahedron Lett.*, **51**, 1103 (2010).
28. C. K. Maurya, U. Pathak and P. K. Gupta, *Anal. Bioanal. Chem.*, **413**, 4501 (2021).
29. Y. Liu, X. Wang, E. Feng, C. Fan and S. Pu, *Spectrochim. Acta A Mol. Biomol. Spectrosc.*, **246**, 119052 (2021).
30. M. S. Kim, D. Yun, J. B. Chae, H. So, H. Lee, K. Kim, M. Kim, M. H. Lim and C. Kim, *Sensors*, **19**, 5458 (2019).
31. S. Jana, S. Prajapati, K. K. Suryavanshi, S. Goswami, R. Parida and S. Giri, *J. Phys. Org. Chem.*, **33**, 1 (2020).
32. Q. Lin, Y. Q. Fan, P. P. Mao, L. Liu, J. Liu, Y. M. Zhang, H. Yao and T. B. Wei, *Chem. A Eur. J.*, **24**, 777 (2018).
33. J. M. Jung, J. H. Kang, J. Han, H. Lee, M. H. Lim, K. T. Kim and C. Kim, *Sens. Actuators B Chem.*, **267**, 58 (2018).
34. J. H. Kang, J. Han, H. Lee, M. H. Lim, K. T. Kim and C. Kim, *Dyes Pigm.*, **152**, 131 (2018).
35. J. B. Chae, H. Lee and C. Kim, *J. Fluoresc.*, **30**, 347 (2020).
36. J. Sun, T. Li, C. Liu, J. Xue, L. Tian, K. Liu, S. Li and Z. Yang, *J. Photochem. Photobiol. A Chem.*, **406**, 113007 (2021).
37. H. Taş, J. Adams, J. C. Namyslo and A. Schmidt, *RSC Adv.*, **11**, 36450 (2021).
38. N. Mudi, P. Hazra, M. Shyamal, S. Maity, P. K. Giri, S. S. Samanta, D. Mandal and A. Misra, *J. Fluoresc.*, **31**, 315 (2021).
39. H. So, H. Cho, H. Lee, M. C. Tran, K. T. Kim and C. Kim, *Microchem. J.*, **155**, 104788 (2020).
40. F. P. Ying, H. S. Lu, X. Q. Yi, Y. Q. Xu and Y. Y. Lv, *Sens. Actuators B Chem.*, **340** (2021).
41. N. S. Mohamad, N. H. Zakaria, N. Daud, L. L. Tan, G. C. Ta, L. Y. Heng and N. I. Hassan, *Sensors (Switzerland)*, **21**, 1 (2021).
42. S. C. Lee, M. Lee, B. Suh, J. Lee and C. Kim, *ChemistrySelect*, **6**, 8397 (2021).
43. B. K. Rani and S. A. John, *J. Photochem. Photobiol. A Chem.*, **418**, 113372 (2021).
44. M. Wu, D. D. Yang, H. W. Zheng, Q. F. Liang, J. Bin Li, Y. Kang, S. Li, C. Jiao, X. J. Zheng and L. P. Jin, *Dalton Trans.*, **50**, 1507 (2021).
45. A. K. K. Bhasin, P. Chauhan and S. Chaudhary, *Sens. Actuators B Chem.*, **330**, 129328 (2021).
46. C. Jiang, L. Yang, P. Li, Y. Liu, S. Li, Y. Fu and F. Ye, *Spectrochim. Acta A Mol. Biomol. Spectrosc.*, **263**, 120168 (2021).
47. S. Jiang, S. Chen, Z. Wang, H. Guo and F. Yang, *Sens. Actuators B Chem.*, **308**, 127734 (2020).
48. E. Bahojb Noruzi, M. Kheirkhahi, B. Shaabani, S. Geremia, N. Hickey, F. Asaro, P. Nitti and H. S. Kafil, *Front. Chem.*, **7** (2019).
49. K. H. Alharbi, *Crit. Rev. Anal. Chem.*, 1 (2022).
50. Z. Gao, S. Qiu, M. Yan, H. Liu, S. Lu, H. Lian, P. Zhang, J. Zhu and M. Jin, *J. Mol. Struct.*, **1254**, 132312 (2022).
51. A. Jayaraj, M. S. Gayathri, G. Sivaraman and C. A. S. P, *J. Photochem. Photobiol. B Biol.*, **226**, 112371 (2022).
52. S. Paul and P. Banerjee, *Sens. Actuators B Chem.*, **329**, 129172 (2021).
53. Gaussian 16, Revision C.01, M. J. Frisch, G. W. Trucks, H. B. Schlegel, G. E. Scuseria, M. A. Robb, J. R. Cheeseman, G. Scalmani, V. Barone, G. A. Petersson, H. Nakatsuji, X. Li, M. Caricato, A. V. Marenich, J. Bloino, B. G. Janesko, R. Gomperts, B. Mennucci, H. P. Hratchian, J. V. Ortiz, A. F. Izmaylov, J. L. Sonnenberg, D. Williams-Young, F. Ding, F. Lipparini, F. Egidi, J. Goings, B. Peng, A. Petrone, T. Henderson, D. Ranasinghe, V. G. Zakrzewski, J. Gao, N. Rega, G. Zheng, W. Liang, M. Hada, M. Ehara, K. Toyota, R. Fukuda, J. Hasegawa, M. Ishida, T. Nakajima, Y. Honda, O. Kitao, H. Nakai, T. Vreven, K. Throssell, J. A. Montgomery Jr., J. E. P., F. Ogliaro, M. J. Bearpark, J. J. Heyd, E. N. Brothers, K. N. Kudin, V. N. Staroverov, T. A. Keith, R. Kobayashi, J. Normand, K. Raghavachari, A. P. Rendell, J. C. Burant, S. S. Iyengar, J. Tomasi, M. Cossi, J. M. Millam, M. Klene, C. Adamo, R. Cammi, J. W.

Ochterski, R. L. Martin, K. Morokuma, O. Farkas, J. B. Foresman and D. J. Fox, Gaussian, Inc., Wallingford CT (2016).
54. A. D. Becke, *J. Chem. Phys.*, **98**, 5648 (1993).
55. M. M. Francl, W. J. Pietro, W. J. Hehre, J. S. Binkley, M. S. Gordon, D. J. DeFrees and J. A. Pople, *J. Chem. Phys.*, **77**, 3654 (1982).
56. P. C. Hariharan and J. A. Pople, *Theor. Chim. Acta*, **28**, 213 (1973).
57. P. J. Hay and W. R. Wadt, *J. Chem. Phys.*, **82**, 299 (1985).
58. A. Klamt, C. Moya and J. Palomar, *J. Chem. Theory Comput.*, **11**, 4220 (2015).
59. A. M. Brouwer, *Pure Appl. Chem.*, **83**, 2213 (2011).

Supporting Information

A novel fluorescent turn-on probe based on thiosemicarbazide-naphthalene for selectively detecting Zn^{2+}

Minji Lee, Sungjin Moon, Dongkyun Gil, and Cheal Kim†

Department of Fine Chemistry, and New and Renewable Energy Convergence,
Seoul National University of Science and Technology, Seoul 01811, Korea
(*Received 4 January 2023 • Revised 3 March 2023 • Accepted 31 March 2023*)

Table S1. Examples of chemosensors containing thiosemicarbazide derivative for detecting Zn^{2+}

No.	Structure	Detection limit	K value (M^{-1})	Solvent	Water sample	Test strip	Detecting method	Ref.
1	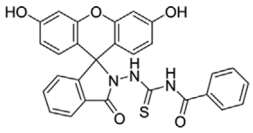	-	-	CH_3CN/H_2O (2 : 8)	-	-	Fluorescence turn-on	[1]
2	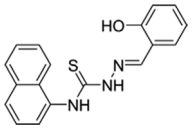	0.50 μM	10^6	$EtOH/H_2O$ (7 : 3)	O	-	Ratiometric fluorescence	[2]
3	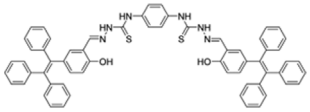	0.08 μM	-	THF/H_2O (1 : 9)	-	O	Fluorescence turn-on	[3]
4	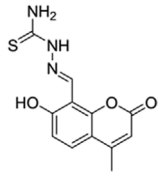	6 nM	2.847×10^3	$EtOH/H_2O$ (8 : 2)	-	O	Fluorescence turn-on	[4]
5	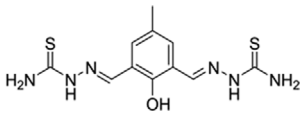	0.15 μM	1.16×10^4	HEPES buffer	O	-	Fluorescence turn-on	[5]
6	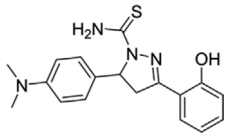	0.93 μM	1.284×10^4	$EtOH/H_2O$ (1 : 1)	-	-	Fluorescence turn-on	[6]
7	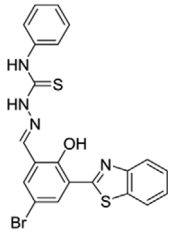	0.39 μM	4.155×10^4	$MeOH/H_2O$ (3 : 2)	-	-	Ratiometric fluorescence	[7]
8	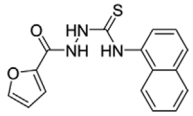	1.93 μM	2.8×10^4	DMF/H_2O (1 : 9)	O	O	Fluorescence turn-on	This work

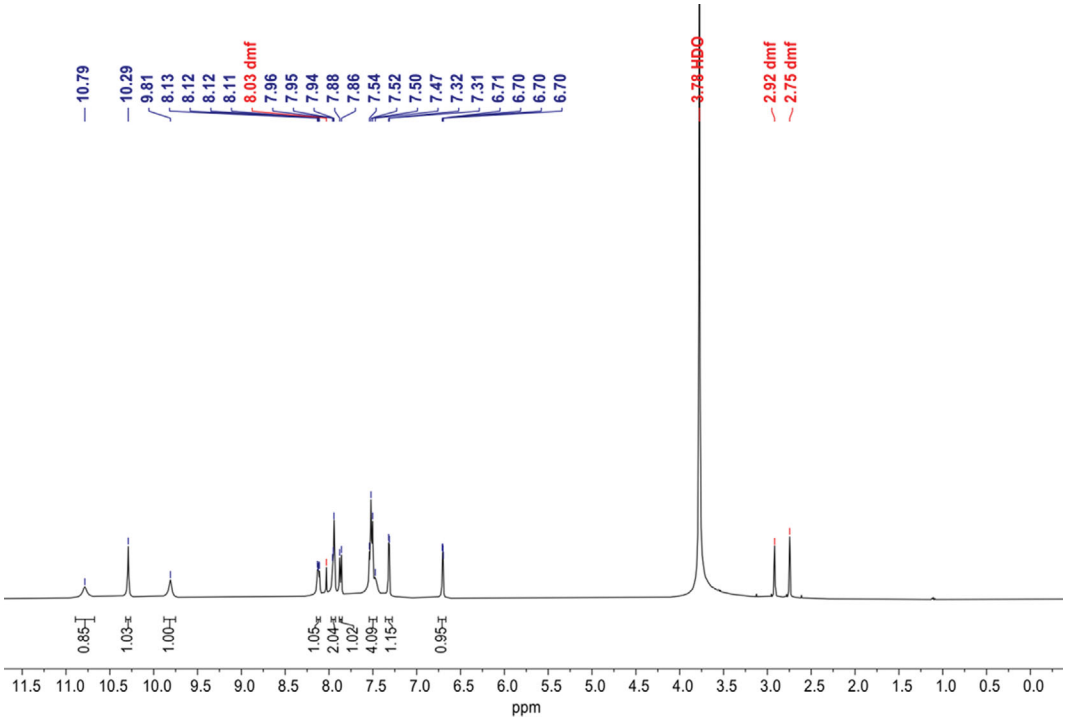

Fig. S1. ^{1}H NMR spectrum of FNC.

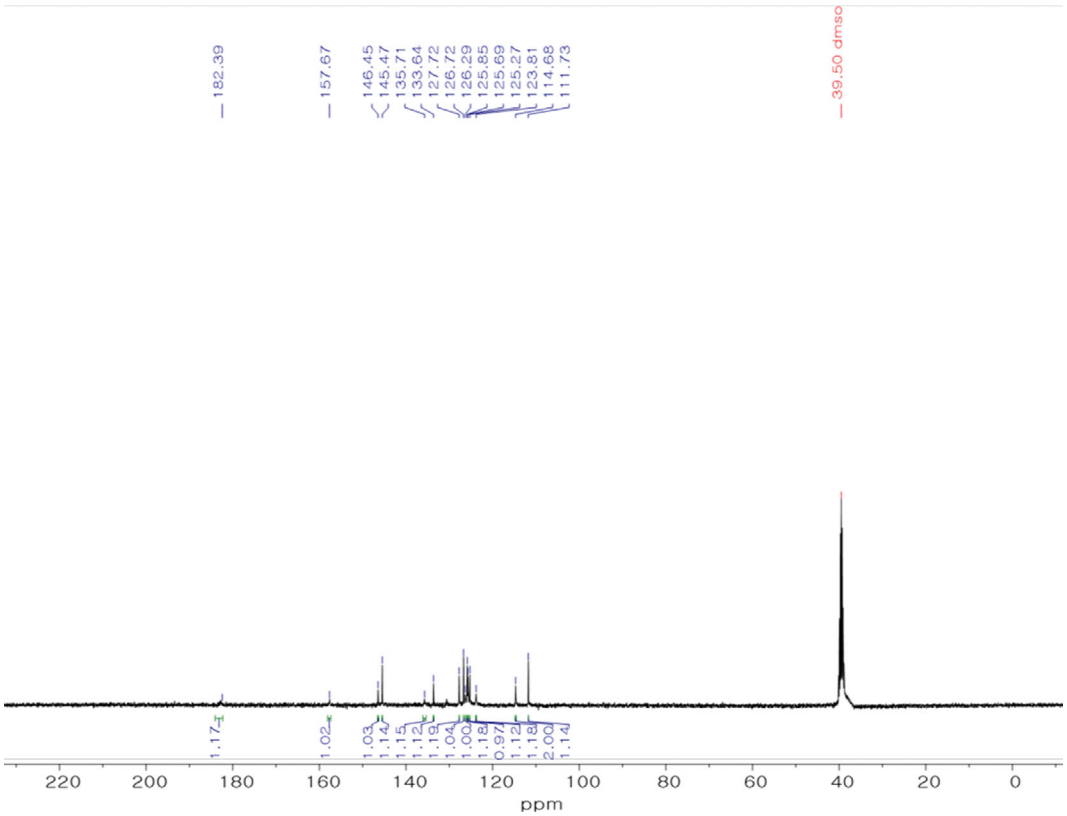

Fig. S2. ^{13}C NMR spectrum of FNC.

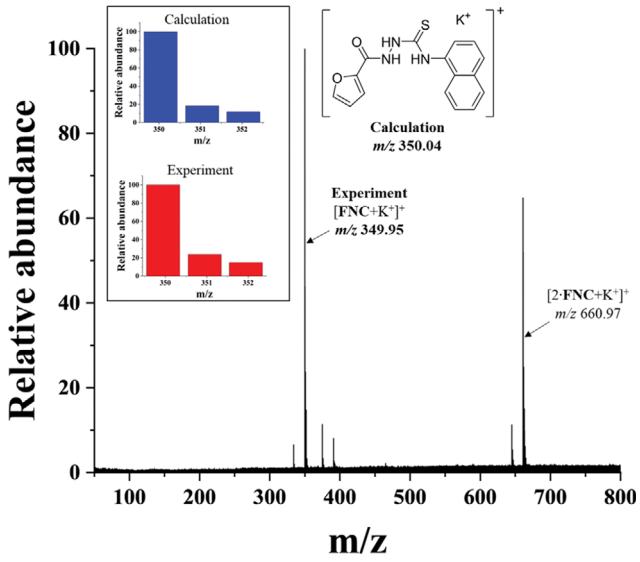

Fig. S3. Positive-ion ESI-mass of FNC.

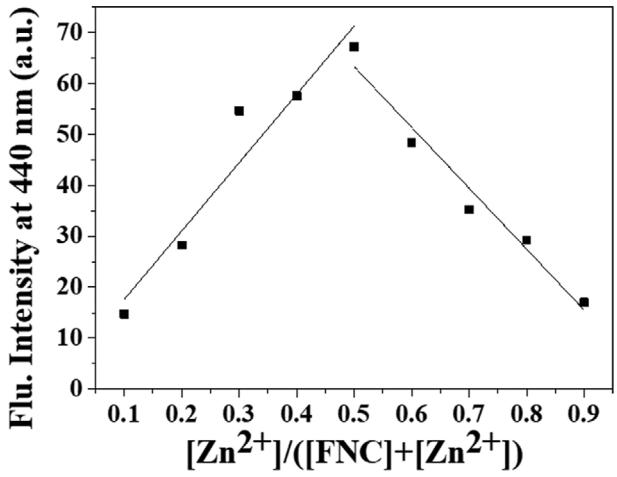

Fig. S4. Job plot for probe FNC and Zn^{2+}.

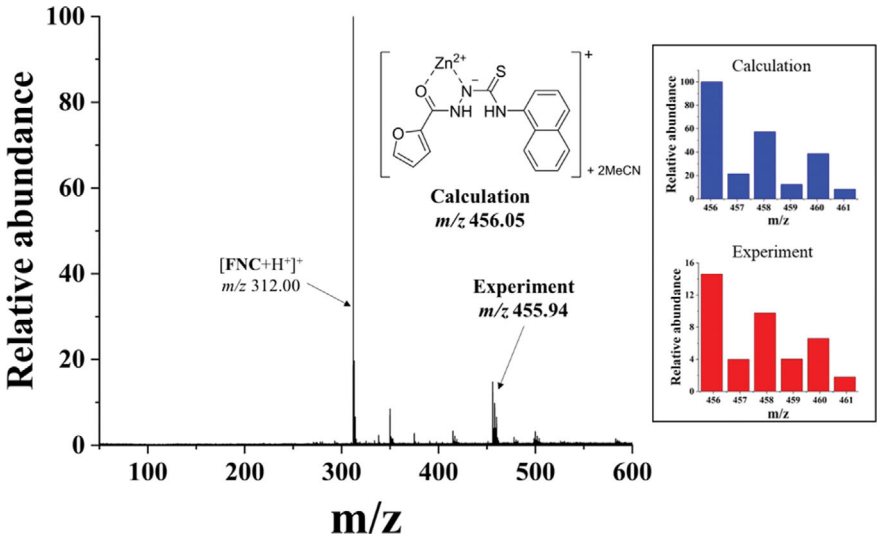

Fig. S5. Positive-ion ESI-mass of FNC with $Zn(NO_3)_2$ (1.0 equiv).

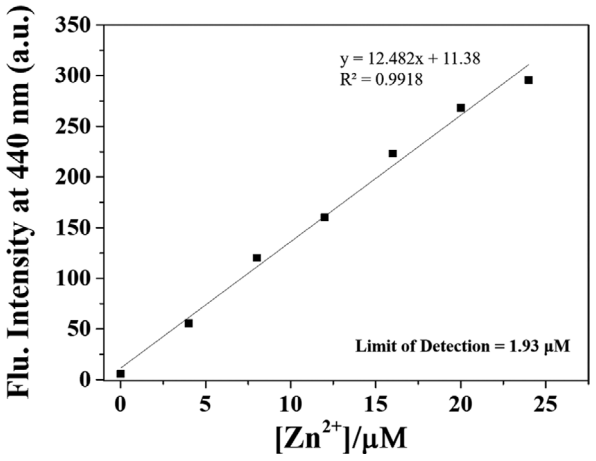

Fig. S6. Limit of detection of FNC for Zn^{2+} determined by the intensity change at 440 nm.

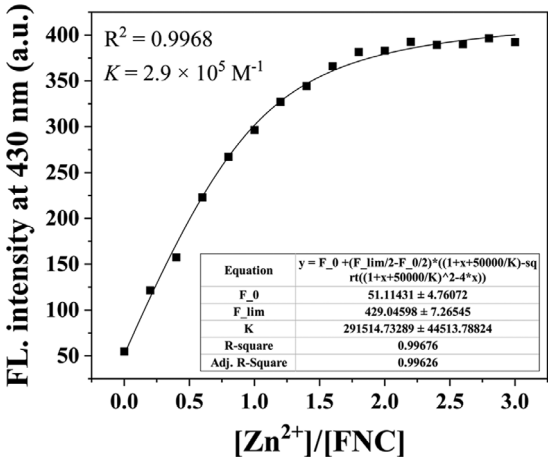

Fig. S7. Determination of the binding constant (K) between FNC (20 μM) and Zn^{2+} based on non-linear fitting.

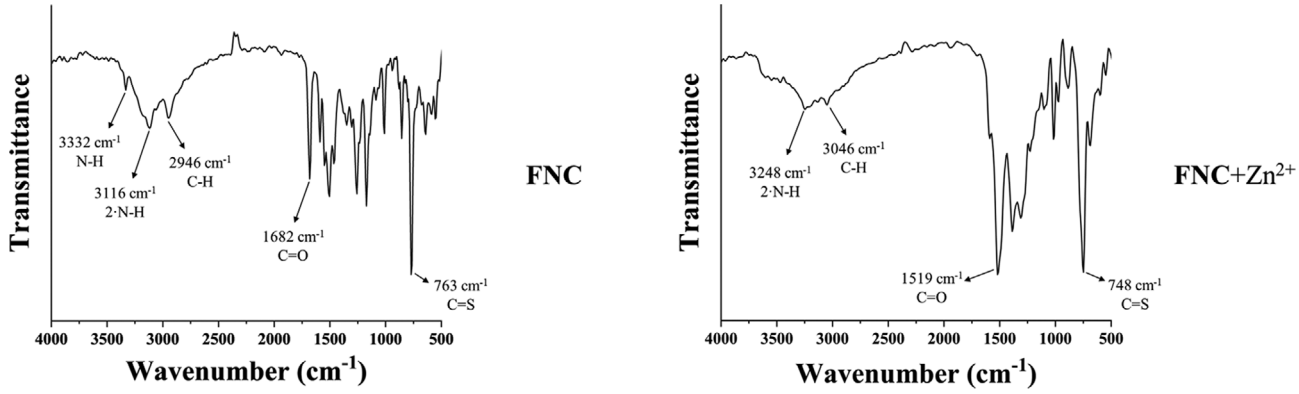

Fig. S8. FT-IR spectra of FNC and FNC-Zn^{2+}.

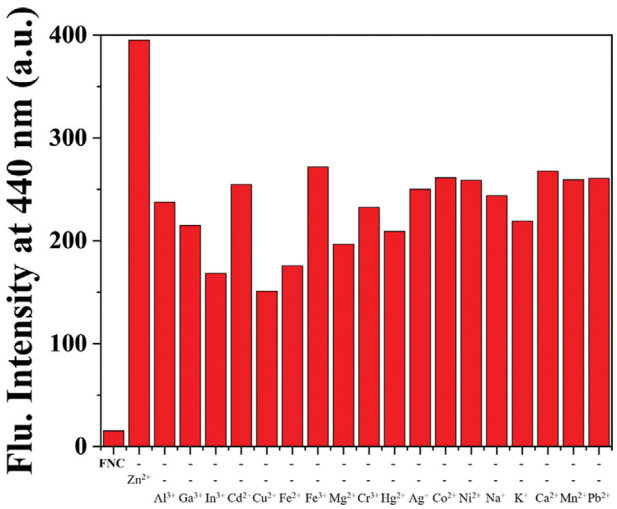

Fig. S9. Competitive test of FNC to Zn^{2+} (3.0 equiv) in the presence of various metal ions.

(a)

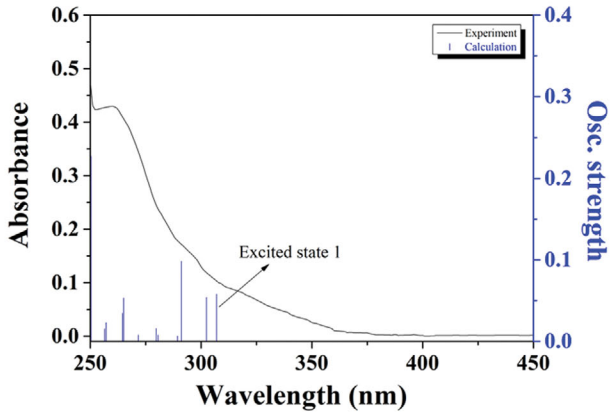

(b)

Excited state 1	Wavelength (nm)	Percent (%)	Main Character	Oscillator strength
H → L H-1 → L	306.95	47 35	ICT, π-π* transiton	0.0541

Fig. S10. (a) The theoretical excitation energies and the experimental UV-vis spectrum of FNC. (b) The major electronic transition energies and molecular orbital contributions of FNC (H=HOMO and L=LUMO).

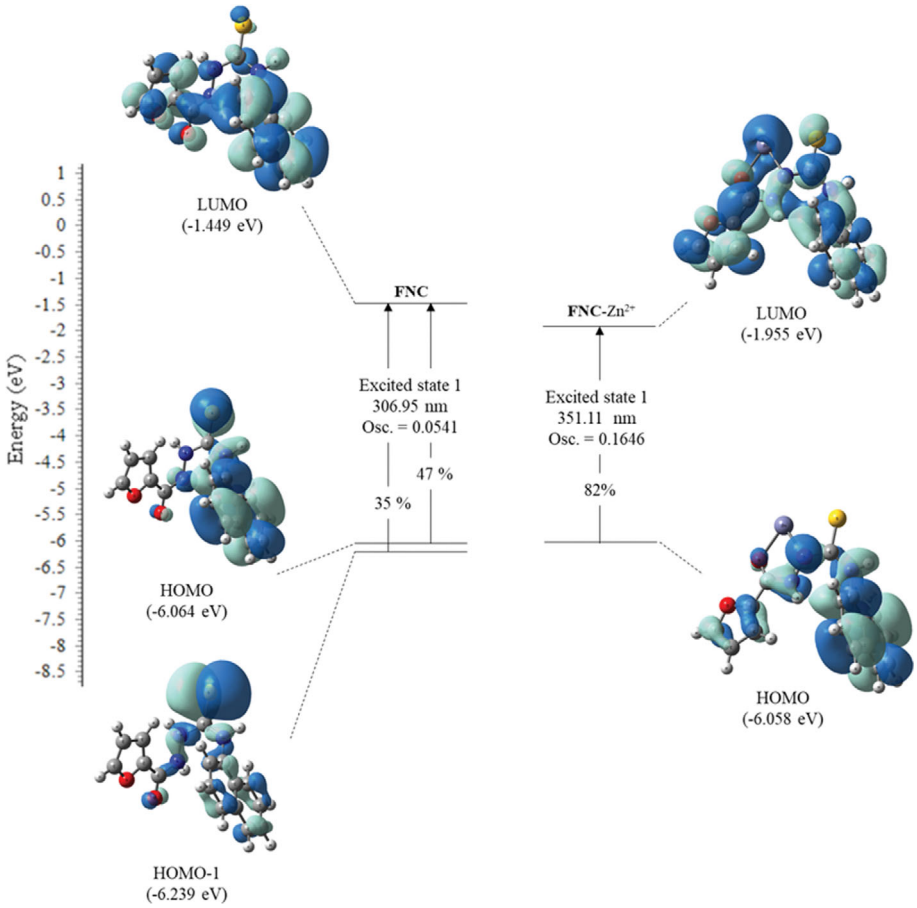

Fig. S11. The major molecular orbital transitions and excitation energies of FNC and FNC-Zn^{2+}.

(a)

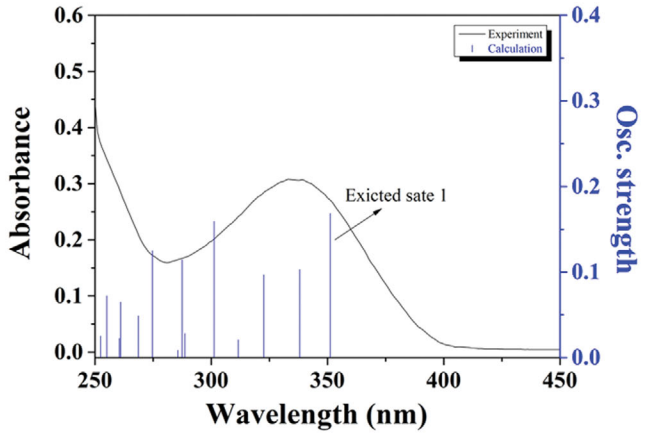

(b)

Excited state 1	Wavelength (nm)	Percent (%)	Main Character	Oscillator strength
H → L	351.11	82	LMCT, π-π* transiton	0.1646

Fig. S12. (a) The theoretical excitation energies and the experimental UV-vis spectrum of FNC-Zn^{2+}. (b) The major electronic transition energies and molecular orbital contributions of FNC-Zn^{2+} (H=HOMO and L=LUMO).

REFERENCES

1. Z. Yang, M. She, B. Yin, L. Hao, M. Obst, P. Liu and J. Li, *Anal. Chim. Acta*, **868**, 53 (2015).
2. Z. Li, Y. Xiang and A. Tong, *Anal. Chim. Acta*, **619**, 75 (2008).
3. S. Jiang, S. Chen, Z. Wang, H. Guo and F. Yang, *Sens. Actuators B Chem.*, **308**, 127734 (2020).
4. L. Wang, W. Li, W. Zhi, Y. Huang, J. Han, Y. Wang, Y. Ren and L. Ni, *Sens. Actuators B Chem.*, **260**, 243 (2018).
5. X. Tang, J. Han, Y. Wang, X. Bao, L. Ni, L. Wang and L. Li, *Spectrochim. Acta - Part A Mol. Biomol. Spectrosc.*, **184**, 177 (2017).
6. Y. P. Zhang, W. Y. Niu, C. M. Ma, Y. S. Yang, H. C. Guo and J. J. Xue, *Inorg. Chem. Commun.*, **130**, 108735 (2021).
7. Q. Wu, L. Feng, J. Bin Chao, Y. Wang and S. Shuang, *Analyst*, **146**, 4348 (2021).